Geodesy and Geodynamics 14 (2023) 15–25

Contents lists available at ScienceDirect

Geodesy and Geodynamics

journal homepage: http://www.keaipublishing.com/geog

The influence of pressure waves in tidal gravity records

Bernard Ducarme

Catholic University of Louvain, Georges Lemaître Centre for Earth and Climate Research (ELI), Louvain-la-Neuve, Belgium

ARTICLE INFO

Article history:
Received 7 October 2021
Received in revised form
21 July 2022
Accepted 24 July 2022
Available online 4 October 2022

Keywords:
Atmospheric pressure waves
Atmospheric pressure correction in tidal records
Atmospheric pressure models ERA5 and MERRA-2

ABSTRACT

For the reduction of atmospheric effects, observed gravity has initially been corrected by using the computed barometric admittance k of the in situ measured pressure, expressed in nms^{-2}/hPa units and estimated by least squares method. However, the local pressure changes alone cannot account for the atmospheric mass attraction and loading when the coherent pressure field exceeds a specific size, i.e., with increasing periodicities. To overcome this difficulty, it is necessary to compute the total atmospheric effect at each station using the global pressure field. However, the direct subtraction of the total gravity effect, provided by the models of pressure correction, is not yet satisfactory for ***S***2 and other tidal components, such as ***K***2 and ***P***1, which include solar heating pressure tides. This paper identifies the origin of the problem and presents strategies to obtain a satisfactory solution.

First, we set up a difference vector between the tidal factors of ***M***2 and ***S***2 after correction of the pressure and ocean tides effects. This vector, hereafter denoted as RES**,** presents the advantage of being practically insensitive to calibration errors. The minimum discrepancy between the tidal parameters of ***M***2 and ***S***2 corresponds to the minimum of the RES vector norm d.

Secondly we adopt the hybrid pressure correction method, separating the local and the global pressure contribution of the models and replacing the local contribution by the pressure measured at the station multiplied by an admittance k_{ATM}.

We tested this procedure on 8 stations from the IGETS superconducting gravimeters network (former GGP network). For stations at an altitude lower than 1000 m, the value of d_{opt} is always smaller than 0.0005. The discrepancy between the tidal parameters of the ***M***2 and ***S***2 waves is always lower than 0.05% on the amplitude factors and 0.025° on the phases. For these stations, a correlation exists between the altitude and the value k_{opt}. The results at the three Central European stations Conrad, Pecny and Vienna are in excellent agreement (0.05%) with the DDW99NH model for all the main tidal waves.

1. Introduction

The atmospheric pressure effect on gravity has been widely investigated in Ref. [1]. At first, the concept of barometric admittance k, expressed in nms^{-2}/hPa units, is introduced. It can be either constant or depending on time and frequency ([2,3]). To account for atmospheric effects, observed gravity is corrected by using the computed barometric admittance of the pressure signal recorded at the station, generally estimated by least squares (LSQ) methods. Although the RMS error $m0$ of a single observation reaches its minimum value, this procedure does not provide satisfactory results for the wave ***S***2. After ocean attraction and loading corrections, the corrected tidal factors should be the same for both waves ***M***2 and ***S***2, as there is no resonance in the semidiurnal tidal band. This is, however, not the case. The amplitude factor of ***S***2 is always too small with respect to ***M***2, and its phase is systematically negative [4]. The phase difference is regionally coherent (Fig. 1). A similar behavior is observed for the couple ***O***1−***P***1, where ***P***1 is the annual modulation of ***S***1, another solar heating tide. These discrepancies require further investigations.

For the amplitude factor, the explanation is obvious and can be found in Ref. [2]: the barometric admittance of the background noise ranges from −2 nms^{-2}/hPa at long periods to

E-mail address: bf.ducarme@gmail.com.

Peer review under responsibility of Institute of Seismology, China Earthquake Administration.

Production and Hosting by Elsevier on behalf of KeAi

https://doi.org/10.1016/j.geog.2022.07.005

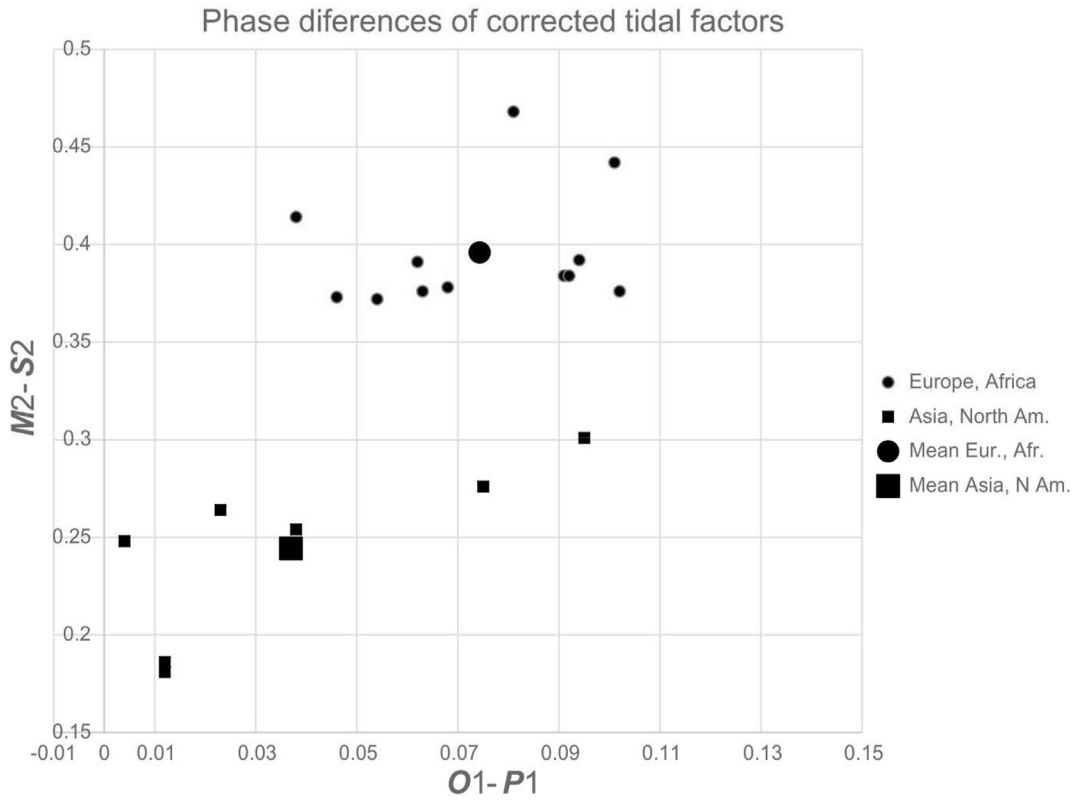

Fig. 1. Phase difference between Lunar and Solar waves (***O***1, ***P***1) and (***M***2, ***S***2).
Circle: Europe (10) + Africa (2), Mean ***O***1-***P***1: 0.074 ± 0.007°, ***M***2-***S***2: 0.396 ± 0.009°.
Square: Asia (4) + North America (3), Mean ***O***1-***P***1: 0.037 ± 0.014°, ***M***2-***S***2: 0.244 ± 0.018°.

about −3.5 nms^{-2}/hPa at periods lower than 8 h, with a phase close to 180°. It explains why the pressure admittance is always close to −3 nms^{-2}/hPa for high pass filtered tidal records. The solar heating tides $\boldsymbol{S}_m$, $m \geq 1$ are more or less planetary waves and have smaller effective admittances. The pressure effect computed from the pressure background is too large for ***S***2 and artificially decreases its amplitude factor.

There is another point to consider. As pointed out by Merriam [5], the local pressure changes alone cannot account for the atmospheric mass attraction and loading when the coherent pressure field exceeds a specific size, i.e., with increasing periodicities. To overcome this difficulty, it is necessary to compute the total atmospheric effect at each station of the worldwide pressure field using surface pressure values on a grid [6] or, as in the most sophisticated models, computing the 3D full effects, where the changes of density with heights are taken into account [7–11]. Ducarme [4] has shown that a global pressure correction approach, based on atmospheric pressure models, was strongly improving the agreement between the amplitude factors of ***M***2 and ***S***2 but was not reducing their observed phase difference at three stations located in Central Europe (Conrad, Pecny and Vienna). This paper presents a new approach to addressing this subsisting issue.

For the analysis of tidal gravity records, we use the latest version ET4-ANA-V80 of the enhanced ETERNA-x software [3,12,13].

2. Pressure spectrum

Chapman and Lindzen [14] provide a general description of atmospheric tides. Besides, Solar waves $\boldsymbol{S}_m$, $m \geq 1$ and a noticeable Lunar wave ***M***2 exists.

Let us first investigate the pressure spectrum. Fig. 2 presents a typical power spectrum for the Membach station. The main pressure waves of order m ($\boldsymbol{S}_m$, $m \geq 1$) are modulated by the complex annual changes of the solar radiation (Fig. 3). Their arguments differ from the main pressure wave of order m by $\pm n(h-p_s)$; h means tropical longitude of the Sun and p_s the mean tropical longitude of the solar perigee. We follow hereafter the notations given in Ref. [15]: modulations are labeled in such a way that $-n(h-p_s)$ is labeled na, and $+n(h-p_s)$ is labeled *nb*. For example, S42a and S42b are the semiannual modulations of ***S***4. In the diurnal (D) and semidiurnal (SD) tidal bands, the arguments of the modulations of the main diurnal (***S***1) and semi-diurnal (***S***2) pressure waves coincide with several main astronomical tidal waves, sometimes within an additional $\pm kp_s$ (Table 1). As the period of the p_s argument is close to 20000 years, it can be considered a constant over several decades, resulting in a constant phase shift between gravity and pressure waves.

Table 1 shows the situation for an equatorial station (Djougou), a mid-latitude station (Membach), and a higher altitude station (Apache Point, $h = 2788$ m). It presents the modulations of $\boldsymbol{S}_a$, ***S***1, and ***S***2 pressure waves in different stations, showing the amplitude of the corresponding gravity wave. The additional correction with respect to the corresponding astronomical wave argument is given between brackets. The spectrum of the stationary pressure waves is quite different in Djougou and Membach [16]. It is clear that the waves ***P***1, PSI1, and PHI1 are impacted in the diurnal band. On ***K***1, the pressure signal is weak. In the semi-diurnal band, ***M***2 is only weakly influenced. A precise determination of the barometric effect in the diurnal band will improve the determination of the liquid core resonance [17]. In the semi-diurnal band, a more precise determination of the tidal parameters will be possible at ***S***2 and ***K***2

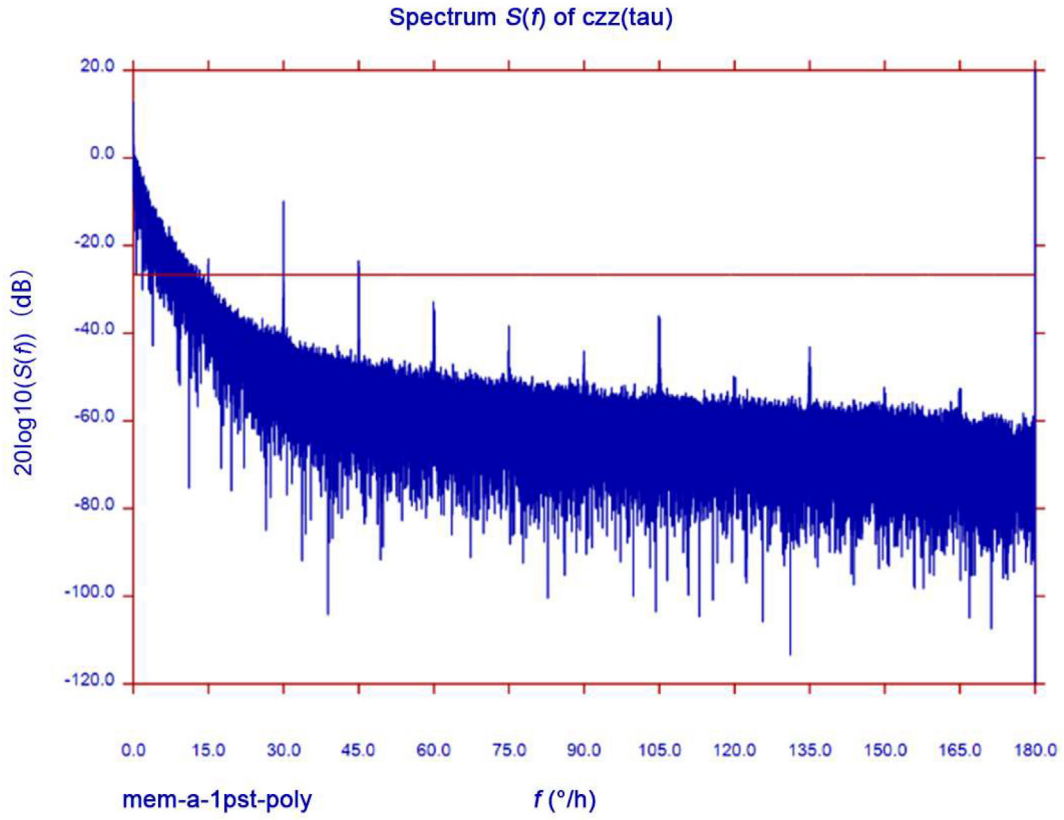

Fig. 2. Typical power spectrum for Membach over the Nyquist frequency interval (hourly sampling).

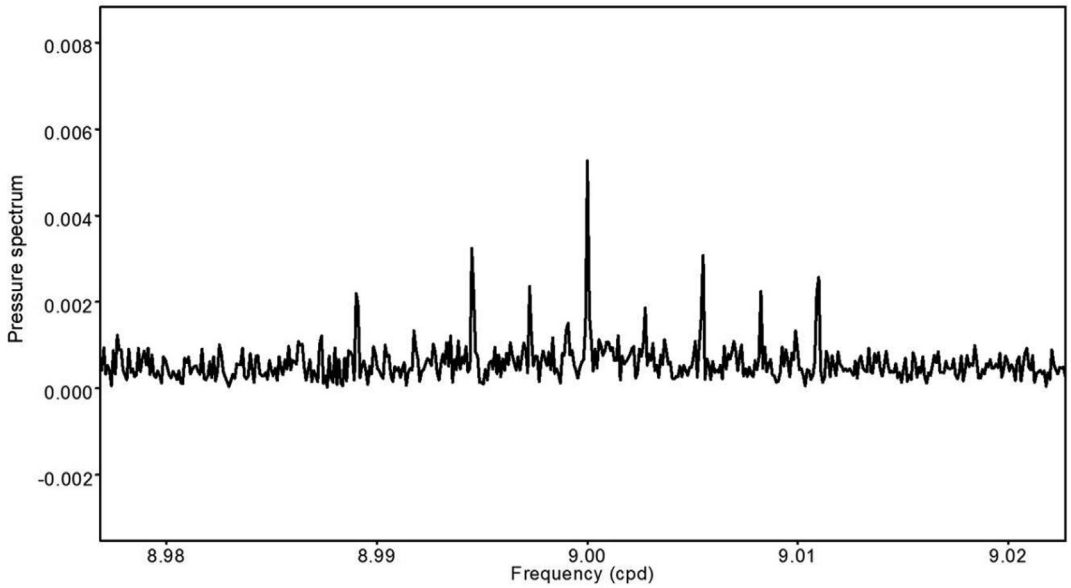

Fig. 3. Pressure spectrum at Membach around ***S***9: from left to right: S94a, S92a, S9a, ***S***9, S9b, S92b, S93b, S94b.

frequencies. In the long period (LP) band, the annual pressure wave and its harmonics are present. Assuming an admittance of -2 nms^{-2}/hPa, the $\boldsymbol{S}_a$ and $\boldsymbol{S}_{ta}$ pressure waves are larger than the astronomical ones in Apache Point.

The pressure spectrum is complex. Degree 3 is questionable due to the shallow water tides [18]. SP3 (3, 3, −4, 0, 0, 0) and SK3 (3, 3, −2, 0, 0, 0) nearly coincide with the annual modulations of ***S***3: S3a (3, 3, −4, 0, 0, 1) and S3b (3, 3, −2, 0, 0, −1). For Membach, both waves are abnormal. At degree 4, the annual modulation S4a coincides exactly with shallow water tide ST4 and the semi-annual modulation S4bb (R4) is very close to shallow water term SK4. The signal-to-noise ratio is better at Membach, where we can

Table 1
Modulations of the pressure waves in the tidal spectrum at different stations.

Gravity	Pressure	Djougou $\varphi = 9.742°$		Apache Point $\varphi = 32.780°$		Membach $\varphi = 50.609°$	
Wave	Modulation	Th. Grav. (nms^{-2})	Pres. (hPa)	Th. Grav. (nms^{-2})	Pres. (hPa)	Th. Grav. (nms^{-2})	Pres. (hPa)
S_a	Annual	4.36	**1.34**	0.59	**4.20**	3.75	0.66
S_{sa}	Semiannual ($-p_s$)	27.47	**0.83**	3.74	**0.99**	23.59	0.50
S_{ta}	Ter-annual ($-p_s$)	1.60	0.35	0.22	0.39	1.38	0.43
Pi1	Semi-annual ($+p_s$)	2.81	0.06	7.69	0.01	8.29	0.01
***P*1**	Annual ($+p_s$)	48.14	**0.19**	131.55	**0.08**	141.83	0.06
***S*1**		1.14	**1.25**	3.11	**0.35**	3.35	0.11
***K*1**	Annual	145.47	0.02	397.53	**0.11**	428.6	0.04
PSI1	Semiannual ($-p_s$)	1.14	**0.07**	3.11	0.01	3.36	0.03
PHI1	Ter-annual ($-3p_s$)	2.07	0.04	5.66	0.02	6.10	0.03
***M*2**		728.95	**0.07**	531.12	**0.03**	302.79	0.01
2***T*2**	Semiannual	0.80	0.03	0.59	0.01	0.33	0.02
***T*2**	Annual	19.82	**0.15**	14.44	**0.06**	8.2	**0.03**
***S*2**		339.12	**1.33**	247.08	**0.58**	140.86	**0.33**
***R*2**	Annual	2.83	**0.03**	2.06	**0.03**	1.18	0.01
***K*2**	Semiannual ($-2p_s$)	92.13	**0.10**	67.13	**0.05**	38.28	**0.04**
K2b	Ter-annual ($-2p_s$)	0.72	0.02	0.52	0.00	0.30	0.0

Note: The argument of the modulations of the pressure waves ***S***a, ***S***1, and ***S***2 can differ of $\pm kp_s$ from the argument of the corresponding tidal gravity waves. Amplitudes in bold correspond to a signal-to-noise ratio larger than 20 dB in the pressure signal.

detect $\boldsymbol{S}_m$ waves up to degree 12, showing a very complex modulation pattern (Fig. 3).

Considering that the astronomical tides have a negligible influence on $\boldsymbol{S}_m$, $m > 2$, we can directly deduce the barometric coefficients $k = k(\boldsymbol{S}_m)$ as the ratio between the amplitude of a specific wave in the gravity records and its amplitude at the same frequency in the pressure record if ocean attraction and loading effect is negligible. We compare the results obtained at Djougou, an equatorial station with large pressure waves, with those of a typical mid-latitude station Membach, where the signal-to-noise ratio remains excellent for large values of m (Table 2).

As the spectrum is generally rich around the main $\boldsymbol{S}_m$ frequency, we also compute a weighted mean $|k|$ for each order (Table 2). In order to avoid dealing with artefacts, we only keep spectral peaks with a phase difference between gravity effect and exciting pressure comprised between 175° and 185°. The signal-to-noise ratio of the pressure components taken into account is rather stable (around 20 db), as the amplitude decrease of the peaks with increasing order is counterbalanced by the corresponding decrease of the background noise. Fig. 4 shows that a linear dependence exists between the barometric coefficient $|k|$ and the order m, at least up to order 10. The RMS error of the regression is 0.1 nms^{-2}/hPa. It is thus possible to extrapolate its value at ***S***2 frequency: 2.25 for Djougou, 2.34 for Membach with a mean value of 2.30.

To check this result, we perform tidal analyses with different values of k until we get equal values of δ_c (***M***2) and δ_c (***S***2). The

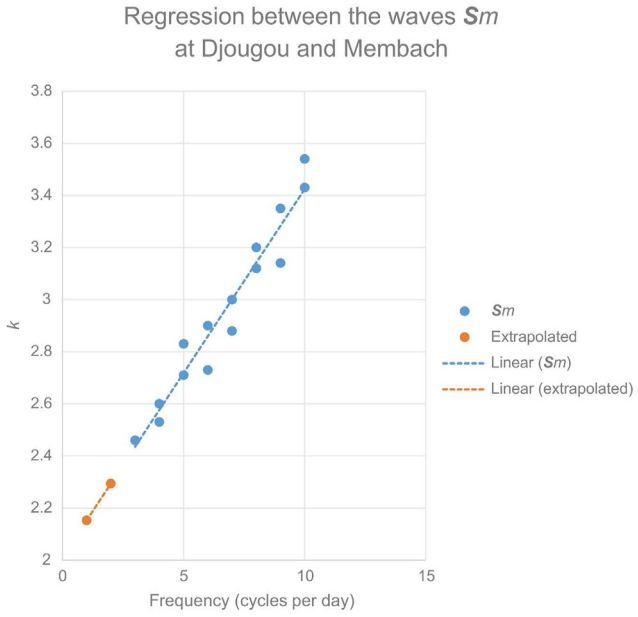

Fig. 4. Linear regression between the station pressure coefficient $|k|$ and the order m of the planetary pressure waves $\boldsymbol{S}_m$.

Table 2
Mean pressure coefficients $|k|$ for increasing harmonic orders of the pressure waves.

Order	DJOUGOU				MEMBACH			
	n	Waves	$\|k\|$ (nms^{-2}/hPa)	RMS-k (nms^{-2}/hPa)	n	Waves	$\|k\|$ (nms^{-2}/hPa)	RMS-k (nms^{-2}/hPa)
3	2	SP3, SK3	2.46	0.19	3	***S*3**	2.46	0.20
4	5	***T*4**, S4a, ***S*4**, S4b, ***R*4**	2.60	0.18	5	***T*4**, S4a, ***S*4**, S4b, ***R*4**	2.60	0.18
5	3	S5a, ***S*5**, S5b	2.83	0.30	1	***S*5**	2.71	0.29
6	3	S6a, ***S*6**, S6b	2.73	0.25	2	S6a, S6b	2.90	0.40
7	4	S73a, S7a, ***S*7**, S73b	2.88	0.28	2	S73a, S73b	3.00	0.12
8	2	S83a, ***S*8**	3.20	0.65	5	S84a, S8a, ***S*8**, S84b	3.12	0.37
9	2	S9a, S9b	3.35	0.71	6	S94a, S92a, S9a, ***S*9**, S92b, S94b	3.14	0.20
10	1	***S*10**	3.54		2	S103a, S103b	3.43	0.30

Note: n - number of waves included in the evaluation of $|k|$.

agreement is found for $k = -2.0$ nms^{-2}/hPa at Djougou and $k = -2.2$ nms^{-2}/hPa at Membach. It means that the pressure contribution to the amplitude of the ***S***2 tide has been correctly removed with this value of k. This result agrees with the values extrapolated from the pressure waves of order m, with $m > 2$ (Fig. 4).

3. Definition of the different constituents of the tidal signal

In tidal gravity analysis, we have access in the time domain to tidal gravity observation series $o(t)$, station pressure data $p(t)$, and eventually auxiliary channels $r(t)$, such as water table measurements. The gravity effect of global atmospheric pressure models is also available as time series $g(t)$. Corrections in the tidal analysis procedure can be performed either in the time domain using auxiliary time series, e.g., pressure, or in the frequency domain on the computed tidal vector, e.g., ocean tides loading.

The results are given in the frequency domain as observed tidal parameters for different waves. The vector diagram of Fig. 5 illustrates this signal environment at a given tidal frequency. The vectors are determined by their amplitude and phase or by means of their amplitude ratio δ and phase difference κ with respect to the theoretical astronomical model (A_{th}, $\kappa_{\mathrm{th}} = 0$).

The observed gravity vector $\boldsymbol{A}_0$ is affected by the calibration error due to the incorrect determination of the transfer function of the tidal gravimeter.

Observed gravity is usually corrected for atmospheric effects during the tidal analysis procedure. In the analysis results, the tidal vector $\boldsymbol{A}(\delta A_{\mathrm{th}}, \alpha)$ is thus already a corrected one.

A simple correction method uses the computed barometric admittance k of the in situ measured pressure $\boldsymbol{P}_{\mathrm{st}}(t)$. This time domain computation procedure is equivalent to subtracting from the uncorrected tidal vector $\boldsymbol{A}_0$ the pressure vector $\boldsymbol{P}_{\mathrm{st}}(P, \pi)$ multiplied by the barometric admittance k. The $\boldsymbol{P}_{\mathrm{st}}$ vector is computed by the LSQ analysis of the pressure signal. To get a correct pressure correction, the k value determined at a global scale (over the whole Nyquist interval) should correspond to its value at the frequency of the considered tidal wave.

$$\boldsymbol{A}(\delta A_{\mathrm{th}}, \alpha) = \boldsymbol{A}_{\mathrm{o}}(\delta_{\mathrm{o}} A_{\mathrm{th}}, \alpha_{\mathrm{o}}) + k\boldsymbol{P}_{\mathrm{st}}(P, \pi)$$

The pressure correction computed using a global atmospheric model $g(t)$ in the time domain is equivalent to adding a correction vector $\boldsymbol{G}(G, \gamma)$ in the frequency domain. This vector is computed by the LSQ analysis of the time series providing the global atmospheric model corrections.

$$\boldsymbol{A}(\delta A_{\mathrm{th}}, \alpha) = \boldsymbol{A}_{\mathrm{o}}(\delta_{\mathrm{o}} A_{\mathrm{th}}, \alpha_{\mathrm{o}}) + \boldsymbol{G}(G, \gamma)$$

Moreover, Fig. 5 shows the links between the observed tidal vector $\boldsymbol{A}_{\mathrm{o}}$ and the body tide vector ET, respectively via ocean, atmosphere and miscellaneous processes, either deterministic or stochastic**.** By far, the largest vector in $\boldsymbol{B}$ is vector $\boldsymbol{L}(L, \lambda)$, representing gravity changes induced by ocean attraction and loading. Correction of ocean attraction and loading defines the vectors

$$\boldsymbol{A}_{\mathrm{c}}(\delta_{\mathrm{c}} A_{\mathrm{th}}, \alpha_{\mathrm{c}}) = \boldsymbol{A}(\delta A_{\mathrm{th}}, \alpha) - \boldsymbol{L}(L, \lambda)$$

and $\boldsymbol{X}(X, \chi) = \boldsymbol{A}_{\mathrm{c}}(\delta_{\mathrm{c}} A_{\mathrm{th}}, \alpha_{\mathrm{c}}) - \mathrm{BT}(\delta_{\mathrm{BT}} A_{\mathrm{th}}, 0)$

$\boldsymbol{A}_{\mathrm{c}}$ would be very close to the body tide model if the ocean model computations are correct and if other important sources of discrepancies like the atmospheric pressure induced gravity $\boldsymbol{G}(G, \gamma)$ are correctly taken into account. In Fig. 5, we neglect the gravity impact $\boldsymbol{R}$ of the set of remaining physical processes $r(t)$ like those from hydrology (groundwater, rainfall, etc.). In most cases, $\boldsymbol{R}$ will not be modeled due to lack of information, although its nature is deterministic. As a consequence, one has to be aware that it will appear as a residual vector component and might bias the statistical quantities derived.

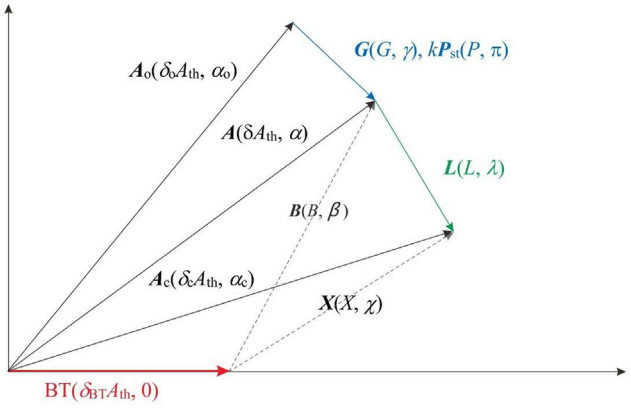

Fig. 5. Earth tide signal representation in the frequency domain: $\boldsymbol{A}_0$ measured signal, $\boldsymbol{A}$ pressure corrected signal, $\boldsymbol{A}_{\mathrm{c}}$ ocean tides loading corrected signal, BT body tides, $\boldsymbol{G}$ pressure correction, $\boldsymbol{P}_{\mathrm{st}}$ station pressure, $\boldsymbol{L}$ ocean tides effect, $\boldsymbol{B}$ tidal residue, $\boldsymbol{X}$ final residue.

4. The difference vector RES

Let us consider the corrected tidal vector $\boldsymbol{A}_{\mathrm{c}}$. As there are no resonance effects in the SD tidal band [17], the tidal Earth models deliver constant amplitude factors and phase shifts equal to 0. Hence, δ_{c} should be the same for ***M***2 and ***S***2, and the phase shifts κ_{c} of both waves should be close to each other. This conclusion is valid under the working hypothesis that the ocean tides attraction and loading contributions on ***M***2 and ***S***2 match correctly. The best correction of the pressure effects should thus correspond to a minimum difference between the corrected tidal factors of ***M***2 and ***S***2.

We can set up the difference vector, hereafter denoted as RES**,** between the ocean and pressure corrected tidal factors of ***M***2 and ***S***2:

$$\mathrm{RES} = \mathrm{FC}_{\boldsymbol{M}2}(\delta_{\mathrm{c}}(\boldsymbol{M}2), \kappa_{\mathrm{c}}(\boldsymbol{M}2)) - \mathrm{FC}_{\boldsymbol{S}2}(\delta_{\mathrm{c}}(\boldsymbol{S}2), \kappa_{\mathrm{c}}(\boldsymbol{S}2)) \quad (1)$$

where $|\mathrm{FC}| = |\boldsymbol{A}|/A_{\mathrm{th}}$.

The link between $\boldsymbol{A}_{\mathrm{c}}$ and BT is achieved by the vector $\boldsymbol{X}(X, \chi)$, representing all processes besides the already reduced pressure effect and ocean impact $\boldsymbol{L}$. Due to the different amplitudes of ***M***2 and ***S***2, the (absolute) vectors $\boldsymbol{X}(\boldsymbol{M}2)$ and $\boldsymbol{X}(\boldsymbol{S}2)$ are difficult to compare. However, if we consider these vectors normalized by their theoretical amplitudes, they become comparable. Considering the relation

$$\boldsymbol{X} = \boldsymbol{A}_{\mathrm{c}} - \mathrm{BT} \quad (2)$$

and the fact that tidal Earth models give the same tidal factors for ***M***2 and ***S***2:

$$\delta_{\mathrm{BT}}(\boldsymbol{M}2) = \delta_{\mathrm{BT}}(\boldsymbol{S}2) \text{ or } \mathrm{BT}(\boldsymbol{M}2)/A_{\mathrm{th}}(\boldsymbol{M}2) = \mathrm{BT}(\boldsymbol{S}2)/A_{\mathrm{th}}(\boldsymbol{S}2)$$

we get a second definition of the RES vector

$$\mathrm{RES} = \boldsymbol{X}\,(\boldsymbol{M}2)\,/A_{\mathrm{th}}(\boldsymbol{M}2) - \boldsymbol{X}\,(\boldsymbol{S}2)\,/A_{\mathrm{th}}(\boldsymbol{S}2) \quad (3)$$

The norm of vector RES has to be minimized by selecting appropriate values for the associated pressure correction vector $\boldsymbol{G}$.

As a matter of fact, vector RES is only weakly impacted by calibration errors in amplitude and phase. For example, the phase difference between ***M***2 and ***S***2 is only 0.01° for a largely exaggerated error of 30 s in the instrumental time lag determination. An error in the calibration factor affects the amplitude factors of all the waves in the same way. We can write

$$\begin{aligned}\mathrm{RES} = {} & \mathrm{FC}_{\boldsymbol{M2}}(\delta_c(\boldsymbol{M2})\,(1+\varepsilon),\,\kappa_c(\boldsymbol{M2})) \\ & -\mathrm{FC}_{\boldsymbol{S2}}(\delta_c(\boldsymbol{S2})\,(1+\varepsilon),\,\kappa_c(\boldsymbol{S2}))\end{aligned} \tag{4}$$

where the absolute calibration error ε is the norm of the calibration error vector $\boldsymbol{\epsilon}_{\mathrm{obs}}$.

Then, the norm of the difference vector RES(***M***2, ***S***2) is

$$|\mathrm{RES}| = (1+\varepsilon)\sqrt{[\delta_c(\boldsymbol{M2})\cos\kappa_c(\boldsymbol{M2}) - \delta_c(\boldsymbol{S2})\cos\kappa_c(\boldsymbol{S2})]^2 + [\delta_c(\boldsymbol{M2})\sin\kappa_c(\boldsymbol{M2}) - \delta_c(\boldsymbol{S2})\sin\kappa_c(\boldsymbol{S2})]^2} \tag{5}$$

For a relative calibration error of 0.2% ($\varepsilon = 0.002$ absolutely), the norm of the vector is affected by the same relative error. As the norm of RES is only very slightly dependent on calibration errors, the minimum value of RES should thus correspond to the best correction of the pressure effects at ***S***2 frequency.

Let us now consider the magnitude of the pressure effects on ***M***2 and ***S***2. For the stations of Membach and Djougou, we get the following orders of magnitude:

- Considering the maximum variation of ***M***2 corrected tidal parameters due to pressure fluctuations, we come up with the following values: Djougou 0.03% in amplitude, Membach 0.01% in amplitude.
- For ***S***2, the variations are much larger: Djougou 0.5% in amplitude and 0.44° in phase, Membach 0.35% in amplitude and 0.32° in phase. The total effect on ***S***2 is thus 1.3% in Djougou and 0.74% in Membach.
- Compared with ***M***2, the pressure effect on ***S***2 is thus 44 times larger in Djougou and 75 times larger in Membach. The ***S***2 pressure term represents 98% of the total effect in Djougou and 99% in Membach.

It follows that RES is completely dominated by ***G***(***S***2).

Let us consider first the value of RES when no pressure correction is applied:

$$\mathrm{RES0} = \mathrm{FC0}_{\boldsymbol{M2}}(\delta 0_c(\boldsymbol{M2}),\,\kappa 0_c(\boldsymbol{M2})) - \mathrm{FC0}_{\boldsymbol{S2}}(\delta 0_c(\boldsymbol{S2}),\,\kappa 0_c(\boldsymbol{S2})) \tag{6}$$

with

$$\mathrm{FC0} = \boldsymbol{A}0_c/A_{\mathrm{th}}$$

$$\boldsymbol{A}0_c = \boldsymbol{A}_o - \boldsymbol{L}$$

If we apply a pressure correction proportional to the observed station pressure $\boldsymbol{P}_{\mathrm{st}}$, we get

$$\begin{aligned}\mathrm{RES} = {} & \mathrm{RES0} + k(\boldsymbol{P}_{\mathrm{st}}(\boldsymbol{M2})/A_{\mathrm{th}}(\boldsymbol{M2}) - \boldsymbol{P}_{\mathrm{st}}(\boldsymbol{S2})/A_{\mathrm{th}}(\boldsymbol{S2})) \\ \cong {} & \mathrm{RES0} - k\cdot\boldsymbol{P}\mathrm{st}(\boldsymbol{S2})/A_{\mathrm{th}}(\boldsymbol{S2})\end{aligned} \tag{7}$$

as ***S***2 pressure effect represents 98% of the total pressure effect.

When k is changing (Fig. 6), the tip of the RES vector moves along a straight line of the equation:

$$y = ax + b \tag{8}$$

where $\alpha = a\tan(a)$ slope, b is ordinate at the origin.

The geometry of this straight line is discussed in the Appendix A. Defining d as | RES |, the minimum value d_{opt} is the distance between the origin and the straight line.

5. Introduction of global pressure models

Global pressure models have been in use for a long time [6,7,19].

We shall shortly present the ERA5 and MERRA-2 models, used by the School and Observatory of Earth Sciences (EOST) Loading Service (http://loading.u-strasbg.fr/GGP/atmos/) to provide the pressure field correction for surface gravity. The ERA5 and MERRA-2 time series, computed on an hourly basis, assume an inverted barometer response for the ocean and have been available since 1980. We use the EOST facilities in this work.

5.1. History of models ERA5 and MERRA-2

As the first model, we use the European Centre for Medium Range Weather Forecasts (ECMWF) latest reanalysis ERA5 of hourly surface pressure. ERA5, generated at Copernicus Climate Change Service (C3S, 2017) [20], provides hourly estimates of a large number of atmospheric, land, and oceanic climate variables. The data cover the Earth on a 30 km grid and resolve the atmosphere using 137 levels from the surface up to 80 km. ERA5 includes uncertainties for all variables at reduced spatial and temporal resolutions. The atmospheric gravity loading is computed using ECMWF operational and reanalysis (ERA interim) pressure data, assuming either an inverted barometer response of the oceans or a dynamic response using HUGO-m [21]. The use of the HUGO-m model has shown significant improvement in terms of reduction of the amplitude of the gravity residuals compared to the classical inverted barometer assumption [6].

The “Modern-Era Retrospective analysis for Research and Applications, version 2 (MERRA-2)” is a global atmospheric reanalysis produced by the NASA Global Modelling and Assimilation Office (GMAO) [22]. It spans the satellite observing era from 1980 to the present. The goals of MERRA-2 are to provide a regularly-gridded, homogeneous record of the global atmosphere and to incorporate additional aspects of the climate system, including trace gas constituents (stratospheric ozone) and improved land surface representation, and cryospheric processes.

The EOST database provides 3 quantities in the ERA5 and MERRA-2 model series:

1. A “local” contribution modl(t) (integration within 0.10° or 0.25° around the gravimeter) using nominal admittances of −2.2105 nms^{-2}/hPa (radius of 0.10°) and −3.0668 nms^{-2}/hPa (radius of 0.25°): eral(t), merl(t);
2. A “non-local = global” contribution modg(t): erag(t), merg(t);

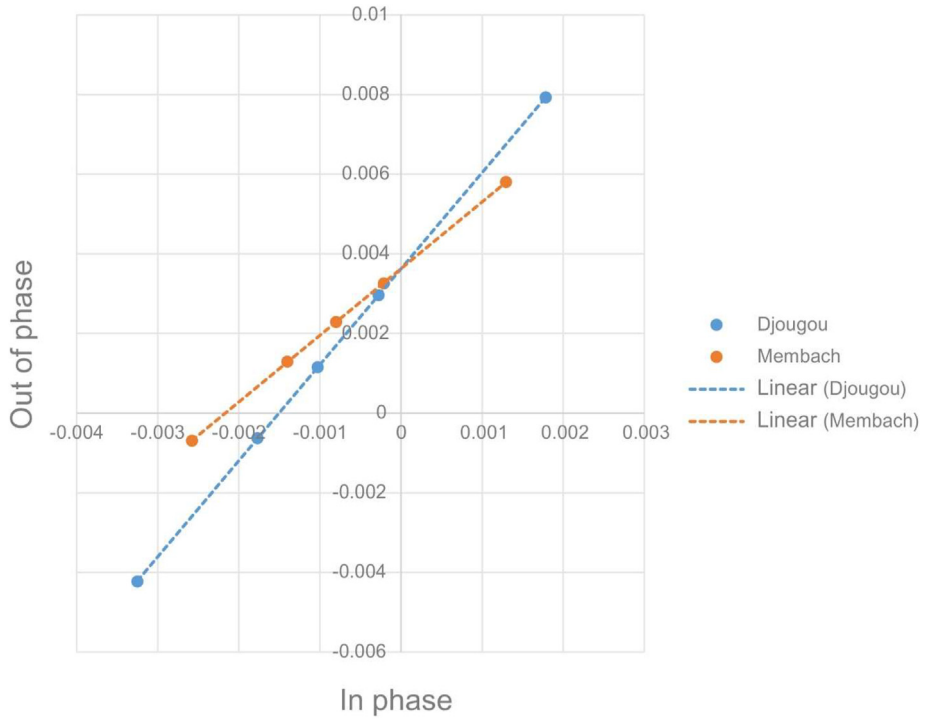

Fig. 6. Linear dependence of the RES vector components for Djougou and Membach stations. Each point represents the tip of the RES vector for a given value of k: from left to right: 0, −1, −1.5, −2, −3.3 (nms^{-2}/hPa).

3. The sum of the previous two, i.e., the total attraction and loading model: modt(t): erat(t), mert(t).

We choose a 0.25° radius for the local contributions in both models.

These quantities represent gravity corrections. The corresponding time series are combined with the superconducting gravimeter observations, i.e., gravity changes $o(t)$ and observed station pressure pst(t).

5.2. Interrelations between model series and station pressure

The linear regression between local contributions and station pressure at Membach provides the following results where r represents the correlation coefficient of the regression

$$\mathrm{eral}(t) = (-3.131 \pm 0.003)\ \mathrm{nms}^{-2}/\mathrm{hPa}\cdot\mathrm{pst}(t),\ r = -0.977$$

$$\mathrm{merl}(t) = (-2.757 \pm 0.004)\ \mathrm{nms}^{-2}/\mathrm{hPa}\cdot\mathrm{pst}(t),\ r = -0.951$$

The pressure admittance computed for the eral channel is close to the value −3.0668 nms^{-2}/hPa used for the computation of the model. A direct fit of ERA5 with MERRA-2 gives

$$\mathrm{eral}(t) = (1.054 \pm 0.001)\cdot\mathrm{merl}(t),\ r = 0.953$$

$$\mathrm{erag}(t) = (1.051 \pm 0.002)\cdot\mathrm{merg}(t),\ r = 0.934$$

$$\mathrm{erat}(t) = (1.100 \pm 0.002)\cdot\mathrm{mert}(t),\ r = 0.934$$

ERA5 model seems to provide corrections up to 10% larger than MERRA-2.

5.3. Strategies of pressure corrections

The usual pressure correction in tidal analysis with the help of local pressure measurements $\boldsymbol{P}_{\mathrm{st}}$ and the barometric admittance (a simple transfer function between pressure and gravity, both measured locally) do not allow an adequate estimation of atmospheric loading [5,23]. One drawback of this approach is that the LSQ approach fits the background pressure noise providing values of k close to −3 nms^{-2}/hPa, far from the value corresponding to the planetary wave $\boldsymbol{S}2$ (section 2). Moreover, the station pressure alone does not provide enough information to model the global pressure waves. It is necessary to introduce the atmospheric pressure models presented above.

A direct application of the models is the use of the total computed attraction and loading effect modt(t) (erat(t) or mert(t)). The time series modt(t) is directly added to the gravity signal before the global adjustment. However, the station pressure provides a more detailed picture of the pressure variations around the station. It is thus interesting to replace modt(t) with the association of the global model modg(t) and the station pressure pst(t) [16]. It is known as the “hybrid” pressure correction method.

At the correction o(t) + modg(t) in the time domain corresponds, in the frequency domain, the replacement of vector RES0 by the vector

$$\mathrm{RES0}_{\mathrm{mod}} = \mathrm{RES0} - \boldsymbol{R}_{\mathrm{mod}} \tag{9}$$

$$\boldsymbol{R}_{\mathrm{mod}}\ (R_{\mathrm{mod}},\ \rho_{\mathrm{mod}}) = \mathrm{Glob}_{\mathrm{mod}}/A_{\mathrm{th}}(\boldsymbol{S}2)$$

$\mathrm{Glob}_{\mathrm{mod}}$ is the contribution of modg(t) at $\boldsymbol{S}2$ frequency (included in $\boldsymbol{G}(G,\ \gamma)$ in Fig. 5)

The vector $\boldsymbol{P}$ is thus simply translated along the strike of a quantity (Appendix A)

$$\Delta d = R_{\mathrm{mod}} \cdot \sin(\pi + \rho_{\mathrm{mod}} - \alpha) \quad (10)$$

5.4. Application of the hybrid pressure correction method

In addition to the 3 stations already considered, we apply the hybrid correction method to the 3 European stations Vienna, Pecny, and Conrad previously studied in Ref. [4].

In Table 3 we present the results obtained with different pressure correction methods: station pressure pst(t) with barometric admittance k, ERA5 total contribution (erat(t)), MERRA-2 total contribution (mert(t)) and optimized hybrid MERRA-2 "global contribution" + station pressure (merg(t)+kpst(t)).

We directly compare the corrected tidal parameters of ***M***2 and ***S***2 using their amplitude ratio $\delta_c(\boldsymbol{M}2)/\delta_c(\boldsymbol{S}2)$ and their phase difference $\alpha_c(\boldsymbol{M}2) - \alpha_c(\boldsymbol{S}2)$. The global fit is expressed by the norm d of the RES vector.

As expected, the direct regression using the station pressure gives the largest discrepancy between the ***M***2 and ***S***2 tidal parameters. The large phase difference confirms the results of Fig. 1. The norm of the barometric admittance $|k_{\mathrm{ATM}}|$ is slightly lower at Apache Point, the only high-altitude station. A slow decrease of $|k_{\mathrm{ATM}}|$ with altitude is observed for the European stations.

A simple reduction using the total atmospheric effect erat(t) or mert(t) significantly decreases the RES vector. An increase of d with the altitude of the station is clearly observed, and in Apache Point d is larger with the global atmospheric models than with the station pressure reduction.

MERRA-2 always performs slightly better with the "hybrid" correction method than ERA5. It is a reason why we show only MERRA-2 results in Table 3. Except in Apache Point, d_{opt} is lower than 0.0005. The discrepancy between the corrected tidal parameters of the ***M***2 and ***S***2 waves is always lower than 0.05% on the amplitude factors and 0.025° on the phases. In Djougou and Membach, the optimal pressure coefficient k_{opt} applied to the station pressure is close to -2.0 nms^{-2}/hPa. It is compatible with the values extrapolated at ***S***2 frequency for these stations (Fig. 4).

For the 4 European stations, a correlation exists between the value of $|k_{\mathrm{opt}}|$ and the altitude of the station ($r = 0.88$), as shown in Fig. 7. Djougou result is in agreement. It is not true for higher altitude stations such as Lijiang (2435 m), Apache Point (2788 m), and

Table 3
Comparison (***M***2, ***S***2) with different pressure corrections.

Station	Height (m)	pst(t)			erat(t)			mert(t)			merg(t) + pst(t)		
		$\delta_c(\boldsymbol{M}2)/\delta_c(\boldsymbol{S}2)$	$\alpha_c(\boldsymbol{M}2) - \alpha_c(\boldsymbol{S}2)$ (°)	d	$\delta_c(\boldsymbol{M}2)/\delta_c(\boldsymbol{S}2)$	$\alpha_c(\boldsymbol{M}2) - \alpha_c(\boldsymbol{S}2)$ (°)	d	$\delta_c(\boldsymbol{M}2)/\delta_c(\boldsymbol{S}2)$	$\alpha_c(\boldsymbol{M}2) - \alpha_c(\boldsymbol{S}2)$ (°)	d	$\delta_c(\boldsymbol{M}2)/\delta_c(\boldsymbol{S}2)$	$\alpha_c(\boldsymbol{M}2) - \alpha_c(\boldsymbol{S}2)$ (°)	d_{opt}
Vienna	193	1.0016	0.266	0.0057	1.0009	0.069	0.0018	1.0005	0.116	0.0024	0.9997	0.010	0.00037
		$k_{\mathrm{ATM}} = -3.379$ nms^{-2}/hPa									$k_{\mathrm{opt}} = -2.27$ nms^{-2}/hPa		
Membach	250	1.0011	0.287	0.0059	1.0010	0.116	0.0026	1.0009	0.140	0.0030	0.9997	0.012	0.00042
		$k_{\mathrm{ATM}} = -3.279$ nms^{-2}/hPa									$k_{\mathrm{opt}} = -1.91$ nms^{-2}/hPa		
Pecny	534	1.0020	0.284	0.0062	1.0006	0.168	0.0034	1.0015	0.143	0.0034	1.0001	0.005	0.00018
		$k_{\mathrm{ATM}} = -3.243$ nms^{-2}/hPa									$k_{\mathrm{opt}} = -1.85$ nms^{-2}/hPa		
Conrad	1044	1.0020	0.294	0.0064	1.0014	0.185	0.0040	1.0008	0.216	0.0045	0.9996	0.015	0.00050
		$k_{\mathrm{ATM}} = -3.194$ nms^{-2}/hPa									$k_{\mathrm{opt}} = -1.56$ nms^{-2}/hPa		
Djougou	483	1.0015	0.358	0.0081	1.0013	0.209	0.0045	1.0002	0.215	0.0044	0.9999	0.000	0.00014
		$k_{\mathrm{ATM}} = -3.381$ nms^{-2}/hPa									$k_{\mathrm{opt}} = -2.01$ nms^{-2}/hPa		
Apache	2788	1.0008	0.301	0.0062	1.0031	0.396	0.0101	1.0009	0.361	0.0073	0.9999	0.057	0.00133
		$k_{\mathrm{ATM}} = -2.583$ nms^{-2}/hPa									$k_{\mathrm{opt}} = -0.72$ nms^{-2}/hPa		

Note: pst(t): correction with station pressure; erat(t), mert(t): ERA5 or MERRA2 total pressure contribution; erag(t), merg(t): ERA5 or MERRA2 non local contribution; k: barometric admittance; d: norm of RES vector; k_{ATM}: regression with local pressure alone; k_{opt}: value adjusted with hybrid pressure correction.

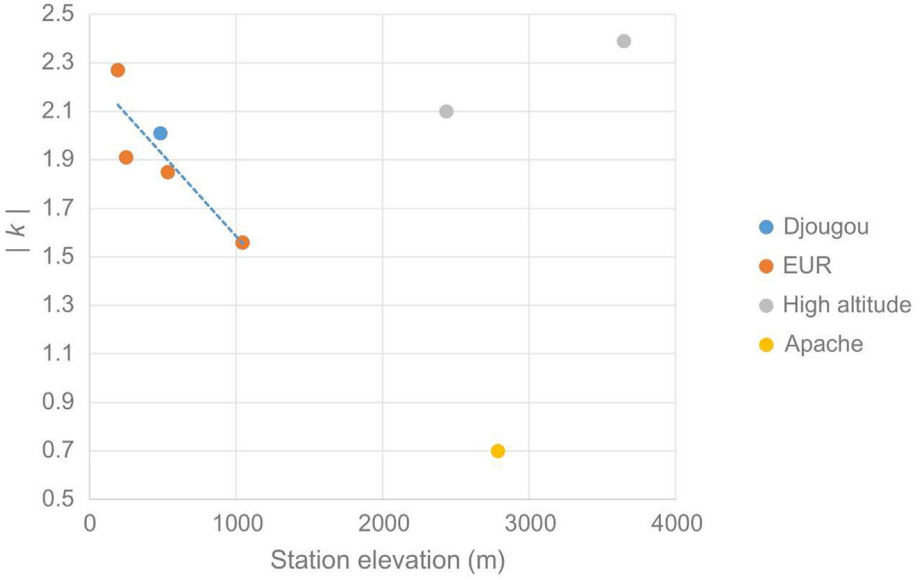

Fig. 7. Correlation between the altitude of the station and the value of k_{opt}. EUR: Vienna, Membach, Pecny, Conrad.

Lhasa (3648 m), shown as grey dots in Fig. 7. The special location of Apache Point station, located on the edge of a cliff [26], could explain the low $|k_{opt}|$ value.

The Djougou station is very interesting due to previous studies of the atmospheric pressure correction [24,25]. We compared our results with those of ANNEX A, Table 4.2.3 in Ref. [16]. The application of our hybrid method on the tidal factors given in Ref. [16], i.e., ***M***2(1.162127, 0.016°), ***S***2(1.16022, −0.170°), provides a vector RES(0.0039, 74°), which is very close to the vector RES(0.0038, 70°) obtained with the admittance $k = -3.0$ nms^{-2}/hPa applied on the station pressure coupled with the global contribution merg(t) of the atmospheric model MERRA2. It should be pointed out that the computation of the ocean attraction and loading effect is different.

It was interesting to study the behavior of the couple (***M***2, ***K***2) at the subtropical station Djougou where the semi-diurnal tides are very large (Th. Grav., in Table 1). The best adjustment for ***K***2 (semiannual modulation of ***S***2) in Djougou confirms the results of ***S***2 ($k_{opt} = -2.0$ nms^{-2}/hPa, $d = 0.0005$). The corrected tidal factors of the 3 waves agree within 0.05% and 0.01°: ***M***2 (1.16075, 0.018°), ***S***2(1.16089, 0.018°), and ***K***2(1.16032, 0.006°).

Finally, we present a vector representation of the effect on ***S***2 of the "local" and "global" corrections of the ERA5 and MERRA-2 models (Table 4). The contribution of the "global" part modg(t) has a small amplitude compared to the contribution of the "local" part modl(t). However, we have seen that the introduction of the "global" part of the model allows reducing drastically the RES vector. In the last column of the Table 4 we compute the effect at ***S***2 frequency of the station pressure multiplied by the barometric admittance $k = -3.0688$ nms^{-2}/hPa, which is the value used in the models for the evaluation of modl(t). We find a very good agreement with the "local" contribution of the models. It explains why the total pressure model modt(t) does not correctly represent the pressure effect at ***S***2 frequency, as the local part modl(t) should use a barometric admittance close to −2.0 nms^{-2}/hPa (Figs. 4 and 7).

6. Revisiting three stations in central Europe

Let us consider now 3 stations located in central Europe: Conrad, Pecny and Vienna [4]. The results of the three stations are very homogeneous with a maximum discrepancy of 0.02% and 0.02° on ***M***2. Table 5 presents the mean corrected tidal factors of the three stations compared with the DDW99NH tidal model [27]. MERRA-2 performs better for ***S***2 (Fig. 8) and all the other tidal waves, except ***P***1. The agreement is always close to 0.05% except for *K*2, but this wave is much smaller than the other main constituents. ***M***2 is only very slightly impacted by the choice of the pressure correction method. This fact justifies retrospectively the use of ***M***2 as a reference in the RES vector. As expected from Table 1, the waves ***P***1 and ***K***1 are also influenced by the pressure correction, but only slightly (<0.05% in amplitude and ≅ 0.05° in phase). In the diurnal band, the pressure corrected observations are fitting very well the DDW99NH model, showing clearly the effects of the liquid core resonance [17].

7. Conclusions

The first goal of this study was to explain why the corrected tidal gravity factors of the wave ***S***2 are systematically different from those of the other semidiurnal waves when a simple barometric admittance k is adjusted during the tidal analysis procedure.

The solar heating tides $\boldsymbol{S}_m$, $m \geq 1$ are more or less planetary waves and have smaller effective admittances than the background noise. As the waves $\boldsymbol{S}_m$, $m \geq 3$ are negligible in the tidal potential, it was possible to derive an effective barometric coefficient dividing the amplitude in the gravity tides records by the amplitude in the atmospheric pressure records. We tested this approach with Djougou and Membach data. A linear dependence exists between the barometric coefficient $|k|$ and the order m, at least up to order 10. It is thus possible to extrapolate its value at ***S***2 frequency: -2.25 nms^{-2}/hPa for Djougou, −2.34 nms^{-2}/hPa for Membach. To confirm this result, we performed tidal analyses with different values of k until we got equal values of δ_c (***M***2) and δ_c(***S***2). We got $k = -2.0$ nms^{-2}/hPa at Djougou and $k = -2.2$ nms^{-2}/hPa at Membach. It means that the pressure contribution to the amplitude of the ***S***2 tide has been correctly removed with this value of k, close to the value extrapolated from the waves $\boldsymbol{S}_m$, $m \geq 3$. The pressure effect, computed over the whole Nyquist interval with values of k close to −3 nms^{-2}/hPa, is thus not correct for ***S***2 and artificially decreases its amplitude factor.

The next step was to present a method to determine the correct tidal parameters for ***S***2. A global pressure correction approach based on atmospheric pressure models ERA5 and MERRA-2 improves the agreement between the amplitude factors of ***M***2 and ***S***2 but does not reduce the observed phase differences. To get better results, we adopt the "hybrid" pressure correction method, separating the "local" and the "global" pressure contribution. We simply

Table 4
Vector representation of the pressure model's contributions at ***S***2 frequency and comparison with station pressure.

Station	A_{th}(***S***2) (nm/s^2)	Global modg(t)				Local modl(t)				Station pressure	
		ERA5		MERRA-2		ERA5		MERRA-2		$k = -3.0668$	
		(nm/s^2)		(nm/s^2)		(nm/s^2)		(nm/s^2)		(nm/s^2)	
Djougou	339	0.95	82°	1.01	93°	4.22	−116°	4.09	−106°	4.08	−114°
Membach	141	0.37	78°	0.40	89°	0.99	−128°	1.04	−119°	1.00	−122°

Table 5
Mean corrected tidal factors of the 3 central European stations (Conrad, Pecny and Vienna) adjusted with different pressure models and the comparison with the DDW99NH model [27]. Rel. diff. = $(\delta_c - \delta_{DDW99NH})/\delta_{DDW99NH}$.

			Station pressure only			Hybrid ERA5			Hybrid MERRA-2		
Wave	Ampl. (nm/s^2)	$\delta_{DDW99NH}$	δ_c	α_c (°)	Rel. diff. (%)	δ_c	α_c (°)	Rel. diff. (%)	δ_c	α_c (°)	Rel. diff. (%)
O1	306	1.15430	1.15358	−0.010	−0.06	1.15358	−0.014	−0.06	1.15357	−0.012	−0.06
P1	142	1.14909	1.14858	−0.023	−0.04	1.14896	0.036	−0.01	1.14871	0.032	−0.03
K1	430	1.13459	1.13520	0.039	0.05	1.13537	0.058	0.07	1.13532	0.060	0.06
M2	312	1.16197	1.16203	0.032	0.01	1.16218	0.032	0.02	1.16210	0.034	0.01
S2	145	1.16197	1.15987	−0.249	−0.18	1.16281	0.003	0.07	1.16236	0.022	0.03
K2	39	1.16197	1.16184	−0.019	−0.01	1.16356	0.030	0.013	1.16321	0.022	0.10

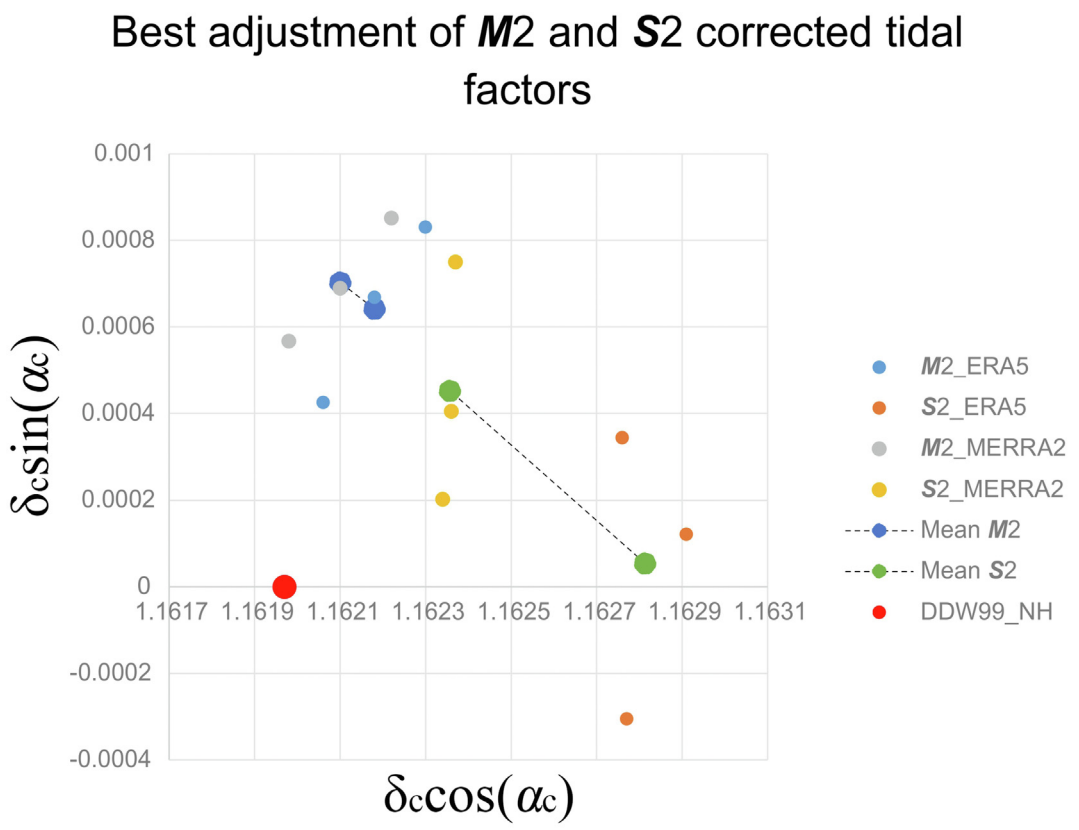

Fig. 8. Adjusted ***M***2 and ***S***2 corrected tidal parameters for Vienna, Pecny, and Conrad stations using a hybrid approach for pressure correction. MERRA-2 results are closer to the reference DDW99_NH model for ***S***2.

replace the "local" contribution of the model with the pressure measured at the station multiplied by a barometric admittance k_{ATM}. As an indicator of the goodness of fit, we set up a difference vector, hereafter denoted as RES, between the corrected tidal factors of ***M***2 and ***S***2. As the ocean tide contribution is well modeled in most non-coastal stations and as there is no resonance in the semi-diurnal band, the vector RES should be very small if the pressure correction is correct at ***S***2 frequency. The RES vector is also practically insensitive to calibration errors. As the tidal factors of the wave ***M***2 are not sensitive to the pressure correction methods, the contribution of ***S***2 represents 98% of the variation of the RES vector. There is a linear dependence of the RES vector with respect to the barometric coefficient k_{ATM} applied to the local pressure measurements.

The best agreement between the corrected tidal parameters of ***M***2 and ***S***2 is obtained with the value k_{opt} corresponding to the minimum value d_{opt} of the RES vector, determined by a trial and error procedure testing different values of k_{ATM}. We extended our study to a total of 8 stations belonging to the IGETS superconducting gravimeters network (former GGP network), using the hybrid pressure correction method and the ERA5 or MERRA-2 models. The MERRA-2 model fits slightly better. For stations at an altitude lower than 1000 m, the value of d_{opt} is always smaller than 0.0005. The discrepancy between the corrected tidal parameters of the ***M***2 and ***S***2 waves is always lower than 0.05% on the amplitude factors and 0.025° on the phases. The values k_{opt} range between -1.5 nms^{-2}/hPa and -2.3 nms^{-2}/hPa and are correlated with the altitude of the station. For two stations in the Himalayas (Lhasa, 3648 m and Lijiang, 2435 m), k_{opt} is close to -2.2 nms^{-2}/hPa. The special location of Apache Point station, located on the edge of a cliff at an altitude of 2788 m, could explain the very weak station pressure influence ($k_{opt} = -0.7$ nms^{-2}/hPa) and a much larger final discrepancy ($d = 0.0013$).

A relevant conclusion is that the direct application of the pressure correction models is not giving correct results for ***S***2. It is due to the fact that the barometric coefficient -3.0668 nms^{-2}/hPa, used for the 0.25° radius inner zone in the global pressure correction models, does not fit at the ***S***2 frequency.

It was important to test whether this pressure correction method is degrading the results of the other tidal waves. The corrected tidal factors at the three Central European stations, Conrad, Pecny, and Vienna, are now in excellent agreement with the DDW99NH model for all the main waves. The discrepancy is only 0.05% except for ***K***2 which is very small in Central Europe.

Conflicts of interest

The authors declare that there is no conflicts of interest.

Acknowledgements

This paper has been prepared in collaboration with Klaus Schueller, who unfortunately passed away in March 2020. He brought a major contribution to the mathematical background of this work. We would like to pay tribute to his deep mathematical literacy that fully expressed itself in the updating of the ETERNA software.

Appendix A. Supplementary data

Supplementary data to this article can be found online at https://doi.org/10.1016/j.geog.2022.07.005.

References

[1] J. Hinderer, B. Hector, J.-P. Boy, U. Riccardi, S. Rosat, M. Calvo, F. Littel, A search for atmospheric effects on gravity at different time and space scales, J. Geodyn. 80 (2014) 50–57.

[2] D.J. Crossley, O.G. Jensen, J. Hinderer, Effective barometric admittance and gravity residuals, Phys. Earth Planet. In. 90 (1995) 221–241.

[3] K. Schueller, Theoretical Basis for Earth Tide Analysis and Prediction, Documentation ET34-X-Vmn, 2019. http://ggp.bkg.bund.de/eterna/.

[4] B. Ducarme, V. Pálinkáš, B. Meurers, Xiaoming Cui, M. Vaľko, On the comparison of tidal gravity parameters with tidal models in central Europe. Proc. 17th Int. Symp. On Earth Tides, Warsaw, 15-19 April 2013. S. Pagiatakis ed. J. Geodyn. vol. 80 (2014) 12–19, https://doi.org/10.1016/j.jog.2014.02.011.

[5] J. Merriam, Atmospheric pressure and gravity, Geophys. J. Int. 109 (1992) 488–500.

[6] J.-P. Boy, P. Gegout, J. Hinderer, Reduction of surface gravity data from global atmospheric pressure loading, Geophys. J. Int. 149 (2009) 534–545, https://doi.org/10.1046/j.1365-246X.2002.01667.x.

[7] J. Neumeyer, J. Hagedoorn, J. Leitloffb, T. Torsten Schmidt, Gravity reduction with three-dimensional atmospheric pressure data for precise ground gravity measurements, J. Geodyn. 38 (2004) 437–450.

[8] J.-P. Boy, B.F. Chao, Precise evaluation of atmospheric loading effects on Earth's time-variable gravity field, J. Geophys. Res. 110 (2005), B08412, https://doi.org/10.1029/2002JB002333.

[9] B. Ducarme, J. Neumeyer, L. Vandercoilden, A.P. Venedikov, The analysis of long period tides by ETERNA and VAV programs with or without 3D pressure correction, Bull. Inf. Marées Terrestres 141 (2006) 11201–11210. http://www.bim-icet.org/.

[10] T. Klügel, H. Wziontek, Correcting gravimeters and tiltmeters for atmospheric mass attraction using operational weather models. New Challenges in Earth's Dynamics – Proceedings of the 16th International Symposium on Earth Tides, December 2009, J. Geodyn. 48 (3–5) (2009) 204–210, https://doi.org/10.1016/j.jog.2009.09.010.

[11] O. Gitlein, L. Timmen, J. Mueller, Modeling of Atmospheric Gravity Effects for High-Precision Observations, Int. J. Geosci. vol. 4 (2013) 663–671, https://doi.org/10.4236/ijg.2013.44061.

[12] H.G. Wenzel, The nanogal software: earth tide data preprocessing package, Bull. Inf. Marées Terrestres 124 (1996) 9425–9439. http://www.bim-icet.org.

[13] K. Schueller, Theoretical basis for Earth Tide analysis with the new ETERNA34-ANA-V4.0 program, Bull.Inf. Marées Terrestres 149 (2015) 12024–12061. http://www.bim-icet.org.

[14] S. Chapman, R.S. Lindzen, Atmospheric Tides, Springer, 1970, ISBN 978-94-010-3399-2.

[15] B. Ducarme, K. Schueller, Canonical wave grouping as the key to optimal tidal analysis, Bull. Inf. Marées Terrestres 150 (2018) 12131–12245. http://www.bim-icet.org/.

[16] J. Hinderer, U. Riccardi, S. Rosat, J.-P. Boy, B. Hector, M. Calvo, F. Littel, J.-D. Bernard, A study of the solid Earth tides, ocean and atmospheric loadings using a 8 year record (2010-2018) from superconducting gravimeter OSG-060 at Djougou (Benin, West Africa), J. Geodyn. 134 (2020), https://doi.org/10.1016/j.jg.o2019.101692.

[17] P. Melchior, The Tides of the Planet Earth, second ed., Pergamo Press, Oxford, 1983.

[18] J.-P. Boy, M. Llubes, R. Ray, J. Hinderer, N. Florsch, S. Rosat, F. Lyard, T. Letellier, Non-linear oceanic tides observed by superconducting gravimeters in Europe, J. Geodyn. 38 (2004) 391–405, https://doi.org/10.1016/j.jog.2004.07.017.

[19] M. Abe, C. Kroner, J. Neumeyer, X.D. Chen, Assessment of atmospheric reductions for terrestrial gravity observations, Bull. Inf. Marées Terrestres 141 (2010) 11201–11210. http://www.bim-icet.org/.

[20] Copernicus Climate Change Service (C3S) ERA5: Fifth Generation of ECMWF Atmospheric Reanalyses of the Global Climate. Copernicus Climate Change Service Climate Data Store (CDS), 2017. https://cds.climate.copernicus.eu/cdsapp#!/home.

[21] L. Carrère, F. Lyard, Modeling the barotropic response of the global ocean to atmospheric wind and pressure forcing – comparisons with observations, Geophys. Res. Lett. 30 (2003), https://doi.org/10.1029/2002GL016473.

[22] R. Gelaro, et al., The Modern-Era retrospective analysis for Research and applications, version 2 (MERRA-2), J. Clim. 30 (2017) 14 5419–5454, https://doi.org/10.1175/JCLI-D-16-0758.1.

[23] A. Mukai, T. Higashi, S. Takemoto, I. Nakagawa, I. Naito, Accurate estimation of atmospheric effects on gravity observations made with a superconducting gravity meter at Kyoto, Phys. Earth Planet. In. 91 (1995) 149–159.

[24] B. Hector, J. Hinderer, L. Séguis, J.-P. Boy, M. Calvo, M. Descloitres, S. Rosat, S. Galle, U. Ricardi, Hydro-gravimetry in West-Africa: first results from the Djougou (Benin) superconducting gravimeter, J. Geodyn. 80 (2014) 34–49, https://doi.org/10.1016/j.jog.2014.04.003.

[25] J. Hinderer, S. Rosat, M. Calvo, J.-P. Boy, B. Hector, U. Riccardi, L. Séguis, Preliminary results from the superconducting gravimeter SG-060 installed in west Africa (Djougou, Benin), in: C. Rizos, P. Willis (Eds.), Earth on the Edge: Science for a Sustainable Planet, International Association of Geodesy Symposia, Springer, BerlinHeidelberg, 2014, pp. 413–419.

[26] D. Crossley, T. Murphy, L. Liang, Comprehensive analysis of superconducting gravimeter data, GPS, and hydrology modeling in support of lunar laser ranging at Apache Point Observatory, New Mexico, Geophys. J. Int. (2022).

[27] V. Dehant, P. Defraigne, J. Wahr, Tides for a convective earth, J. Geophys. Res. 104 (1999) B11035–B11058.

Bernard Ducarme got his Ph.D. degree in Physics in 1973. He worked for 40 years at the Royal Observatory of Belgium in gravimetry and Earth tides. He was Director of the International Centre for Earth Tides between 1999 and 2008. He is an Emeritus Professor at the Catholic University of Louvain.